

Mass-conservation increases robustness in stochastic reaction-diffusion models of cell crawling

Eduardo Moreno and Sergio Alonso*

Department of Physics, Universitat Politècnica de Catalunya, Barcelona, Spain

(Dated: December 30, 2021)

The process of polarization determines the head and tail of single cells. A mechanism of this kind frequently precedes the subsequent cell locomotion and it determines the direction of motion. The process of polarization has frequently been described as a reaction-diffusion mechanism combined with a source of stochastic perturbations. We selected a particular model of amoeboid cell crawling for the motion of *Dictyostelium discoideum* and studied the interplay between pattern formation and locomotion. Next, we integrated the model in a two-dimensional domain considering the shape deformations of the cells in order to characterize the dynamics. We saw that the condition of pattern formation is finely tuned and we propose a modification based on the use of a mass-conservation constraint to substantially increase the robustness of the mathematical model.

Keywords: bistability, stochastic partial differential equations, pattern formation, *dictyostelium discoideum*, cell polarization, amoeboid motion

I. INTRODUCTION

An intensive use of physical and mathematical theories on pattern formation in extended systems [1, 2], gave rise to valuable arguments to explain the formation of certain biological structures. Such mathematical mechanisms have permitted the modeling of processes on very different spatial and temporal scales: from the formation of the skin in fishes [3], to the definition of the direction in embryonic developing [4].

Cell migration is a common phenomenon that is present both in prokaryotic and eukaryotic cells. Living cells migrate to perform different tasks such as food targeting, wound healing and immune response. Independently of the presence of an external signal, before moving, cells need to define the direction to follow. To do so, they first define the front and the back of the cell. The process of formation of a polar direction inside a single cell is commonly known as cell polarization [5] and it is a typical example of pattern formation at the cellular level [6].

Several mathematical models have been developed to explain polarization of single eukaryotic cells [7–9]. Some models rely on a local excitation, which, combined with global inhibition makes the cell respond to external gradients [10], while others rely on the accumulation of a certain biochemical components to guide the motion of the single cells [11]. Normally the accumulation responsible for this second mechanism is combined with a conservation constraint because the process of polarization is fast in comparison to the production of new biochemical components. With this restriction, the mechanism of pattern formation inside living cells to-

gether with the constraint of mass conservation is analogous to a process of coarsening of the initial nucleus of components [12] and gives rise to phase separation [13] and to models of pattern formation [14]. Several simple models of intracellular pattern formation have appeared that include the conservation restriction [11, 15, 16].

Once the axes and direction of movement are defined, in amoeboid cells small projections (defined as protrusions) are formed in the membrane of the cells [17]. These projections, which extend and retract periodically, are responsible for pushing the cell to move in the typical amoeboid motion. *Dictyostelium discoideum* is a species of soil-dwelling amoeba, frequently employed to characterize amoeboid locomotion. Inside the projections of this amoeba, several signaling events are triggered, for example the activation of the Ras proteins and PI3K enzymes and accumulation of PIP_3 at the front of the cell, while activation of PTEN and myosin occur at the rear of the cell [18, 19]. Membrane areas where the protrusion activity is greater are typically characterized by the presence of Ras-GTP protein zones, denoted as patches [20]. The appearance of Ras regions around the membrane with high protrusion activity [10, 21, 22] has been observed in the slime mold organism *Dictyostelium discoideum* where it is related to cytoskeletal dynamics [23].

A reaction-diffusion model with bistable dynamics is one of the common models of cell motility and particularly employed for *Dictyostelium discoideum*. Some dimensional bistable models are based on the formation of a finite lifetime and localized patches of high protein concentration [24, 25] while others are based on membrane dynamics of moving connected points [26]. Bistable conditions for cellular processes can be obtained by the coupling of a mass control regulating condition in the biochemical components present around the cytosol and the membrane of the cell, for example

* Correspondence email address: s.alonso@upc.edu

proteins, phospholipids and enzymes present or other substances in the cytoskeleton [11, 14, 27].

A common technique to model pattern formation inside a cell and the shape evolution of the membrane is the addition of a phase field with a sharp interface to distinguish the interior and exterior of the cell. This field maintains the correct boundary conditions while the borders are moving [28]. Some studies have applied phase field modeling to study keratocyte motility [29–31] and amoeboid motility [32] which can be divided into diffuse and persistent migration depending on the starvation level [33, 34]. There are also some intermediate cases observed in *Dictyostelium discoideum* cells for certain types of genetic variants [35] which have also been modelled with a phase field and variation of some parameters [36–38]. Other properties of *Dictyostelium discoideum* cells modeled employing a phase field are the viscoelasticity of the cells [39] and cell division [40]. Finally, we would like to mention that interactions among cells can also be considered for keratocyte [41, 42] and amoeboid cells [43].

Here, first, we transform a one dimensional model of the polarization at the membrane of a single *Dictyostelium discoideum* cell [21] into a two-dimensional domain for the waves in the basal membrane, in contact with the surface, using an additional phase field for the shape of the cell. We observe a strong dependence of the numerical dynamics on the explicit parameter values of the original model and on the intensity of the stochastic fluctuations. Such dependence indicates that the model is not robust to small variations of the parameters. Therefore, we propose a constraint on the conservation of a component of the signal pathway, controlling the autocatalytic mechanism, in order to increase the robustness of the model in representing changes in parameter values [44]. Similar types of conservation have previously been employed in other models of motion of *Dictyostelium discoideum* cells [32, 36, 45, 46], and we show here that a constraint of this kind is an useful and reasonable condition to systematically increase the robustness of the crawling mechanism, increasing the window of parameter values allowing cell migration.

II. MODEL AND METHODS

A. Biochemical model for Ras activation and pseudopod extension

Biochemical components inside the *Dictyostelium discoideum* amoeba self-organized to follow chemical signals in the exterior by the accumulation of Ras-GTP in the front of the cell. Next, F-actin molecules accumulate also in the front triggering push of the cytoskeleton and the motion of the amoeba.

We investigate a simple reaction-diffusion model [21] for Ras-GTP (R) patches that consists of a local activator and a global inhibitor enhanced by the activation of the Ras-GTP; see diagram in Fig. 1. The partial differential equations employed are:

$$\frac{\partial R}{\partial t} = (1 - R)(k_1 + k_2 \frac{R^{n_1}}{R^{n_1} + K_R^{n_1}} - k_3 G_R - k_4 L_R) - k_5 R \frac{1}{1 + k_6 P} + D_R \nabla^2 R + \xi_R(\vec{x}, t), \quad (1)$$

$$\frac{\partial G_R}{\partial t} = k_7 \langle R \rangle - k_9 G_R, \quad (2)$$

$$\frac{\partial L_R}{\partial t} = (1 - L_R)k_{10}R - k_{11}L_R + D_{LR} \nabla^2 L_R; \quad (3)$$

where $\xi_R(\vec{x}, t)$ is a Gaussian spatio-temporal distributed white noise with zero mean $\langle \xi_R(\vec{x}, t) \rangle = 0$ and correlation $\langle \xi_R(\vec{x}, t) \xi_R(\vec{x}', t') \rangle = 2\sigma_R \delta(\vec{x} - \vec{x}') \delta(t - t')$. The variables L_R and G_R correspond, respectively, to local and global inhibitors of R. Finally, note that the quantity $\langle R \rangle$ corresponds to the spatial integration in the whole system of the field R.

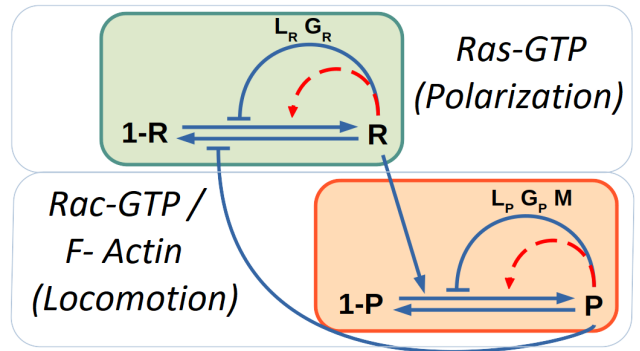


Figure 1. Sketch of the biochemical model of polarization and locomotion modules. Blue solid lines corresponds to the interactions and red dashed lines to auto-catalytic processes. The mass-conservation constraints control the auto-catalytic interactions.

At the same time we included a quantity related to the formation of protrusions (P) such as F-actin and Rac-GTP molecules; see diagram in Fig.1. These variables were coupled with their respective inhibitors:

$$\begin{aligned} \frac{\partial P}{\partial t} = & (1 - P)(k_{12} + k_{13}R + k_{14} \frac{P^{n_2}}{P^{n_2} + K_P^{n_2}}) \\ & + k_{15} \frac{M^{n_3}}{M^{n_3} + K_M^{n_3}} - k_{16}G_P - k_{17}L_P - k_{18}P \\ & + D_P \nabla^2 P + \xi_P(\vec{x}, t), \end{aligned} \quad (4)$$

$$\frac{\partial G_P}{\partial t} = k_{19}\langle P \rangle - k_{20}G_P, \quad (5)$$

$$\frac{\partial L_P}{\partial t} = (1 - L_P)k_{21}P - k_{22}L_P + D_{LP}\nabla^2 L_P; \quad (6)$$

where $\xi_P(\vec{x}, t)$ is a Gaussian spatio-temporal distributed white noise with zero mean $\langle \xi_P(\vec{x}, t) \rangle = 0$ and correlation $\langle \xi_P(\vec{x}, t)\xi_P(\vec{x}', t') \rangle = 2\sigma_P\delta(\vec{x} - \vec{x}')\delta(t - t')$. As in the previous set of equations, the variables L_P and G_P correspond, respectively, to local and global inhibitors of P; while the quantity $\langle P \rangle$ corresponds to the spatial integration in the whole system of the field P.

Finally, the model takes into account the inclusion of a variable of memory (M) which is coupled with P; this variable stimulates the formation of new protrusion zones and represents the results observed in some experiments where a certain relation between the formation of new pseudopods in previous pseudopod locations is present [47, 48]:

$$\frac{\partial M}{\partial t} = k_{23}P - k_{24}M + D_M\nabla^2 M. \quad (7)$$

The memory term is related to the probability of identifying when and where the signaling cascade is activated to generate new pseudopods. At a molecular level, such term is identified with the mechanisms of how information is collected, stored and used to bias future pseudopods [48].

For a more exhaustive description of the model, check the original study [21]. Note that the noise description in the original study was different and we have adapted to an equivalent description based on physical derivations of stochastic fluctuations [49]; for more details see appendix A.

One dimensional simulations were made using periodic boundary conditions and using 120 points for the grid, see an example in Fig.(2,A) where R and P are plotted as function of time. The cell was considered as circular and having a radius of $6.25 \mu m$. The pixel size for this case was set at $\Delta x = 0.32 \mu m$ and the time step $\Delta t = 0.03s$. The definition and the value of the parameters of the model can be found in Table 1 in appendix B.

B. Physical phase field model for cell shape deformations

The original model did not include deformable cells. Therefore, we expanded the model to 2D geometry, see Fig.(2,B) for a simple extension, and coupled it to an auxiliary phase field ϕ with the purpose of describing

the evolution of the cell shape. The use of a phase field permits a smooth variation between the values of $\phi = 1$ inside and $\phi = 0$ outside of the cell, respectively. See an example in Fig.(2,C) where the field P deforms the shape. Note that the fluctuations in P will also affect the shape, see Fig.(2,D).

The phase field equation is the result of a force balance involving several types of forces of different natures acting in the cell body. The equation for the phase field is as follows

$$\tau \frac{\partial \phi}{\partial t} = \gamma \left(\nabla^2 \phi - \frac{G'(\phi)}{\epsilon^2} \right) - \beta \left(\int \phi dA - A_0 \right) |\nabla \phi| + \alpha \phi P |\nabla \phi|, \quad (8)$$

The first term on the right side in eq. (8) is related to the surface energy of the cell membrane, where γ is the surface tension and $G(\phi) = 18\phi^2(1-\phi)^2$ is a double well potential. The second term helps keep the area close to the value of A_0 . And the third term represents the active force generated by the Rac-GTP (P) molecules when pushing on the cell membrane [32].

The inclusion of the phase field as previously mentioned implies a change of geometry from 1D to 2D. Here we consider a deformable cell of $122\mu m^2$ in area corresponding to a circle with radius equal to $6.25\mu m$. The pixel size used was the half as in the 1D case $\Delta x = \Delta y = 0.16\mu m$. Also, to increase accuracy, the time discretization was reduced to $\Delta t = 0.003s$. We integrated Eqs. (1-8) using periodic boundary conditions and standard finite differences. The rest of parameters are as displayed in Table 1 in appendix B.

C. Mathematical description of the mass-conservation constraint

The mathematical model represented in Eqs. (1-7) has several conservation terms which affect the dynamics of the system; see for example Eq.(2) and Eq.(5).

However, we modify the original model to include two new feedback through parameters k_2 and k_{14} to create a more robust model by the control of the bistability properties of the model, which are discussed in following sections. Therefore, the parameters k_2 and k_{14} are dynamically controlled depending on the total amount of the protein R on inducer P at the cell, respectively.

The new control term related to k_2 is

$$k_2 = k_2^* + \eta (\langle R \rangle - C_R), \quad (9)$$

Also, in a similar way, the control term for k_{14} is as follows:

$$k_{14} = k_{14}^* + \eta (\langle P \rangle - C_P), \quad (10)$$

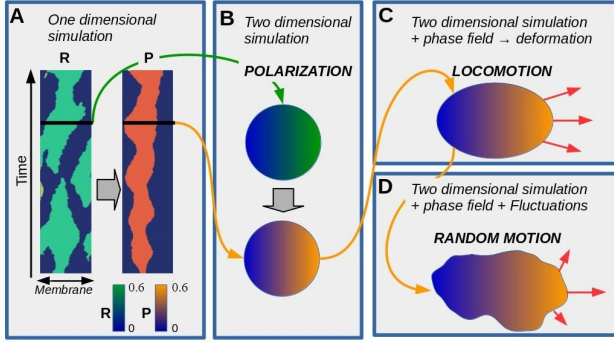


Figure 2. Explanatory box of the modelling techniques. A) Kymograph of a typical one dimensional simulation showing the formation of patches of R and P (horizontal direction corresponds to position in the membrane, and vertical direction to the time evolution). B) Extension to two dimensions with the addition of a circular phase field (Value 1 inside and 0 outside of the circular border). Patches of R and P form in the basal surface of the cell. C) Addition of a dynamic phase field producing the motion and the deformation of the cell. D) Addition of the fluctuations, random two dimensional patches are distributed inside the phase field, driving the motion of the cell.

where k_2^* and k_{14}^* are new constants that take the values of the original value of k_2 and k_{14} , respectively. Note that for $\eta=0$ we recover the original model.

Parameter C_R is the target value of the fraction of the cell area occupied by patches of Ras R . When, the total concentration $\langle R \rangle$ is larger (lower) than C_R the parameter value of k_2 is larger (lower) than k_2^* and the bistable conditions implies the reduction (increase) of the R and, therefore, of $\langle R \rangle$. It corresponds to a feedback control of the parameter to keep a particular stable solution in Eq.(9). The parameter C_P is the target fraction occupied by the pseudopod inducer P and produces an equivalent dynamics on Eq.(10).

III. RESULTS

A. Mechanism of cell motion in the mathematical model is based in stochastic generation of patches

In a one-dimensional system, mimicking the membrane of a crawling cell, the generation of a local patch of high biochemical concentration is equivalent to cell polarization. A stable domain in a specific location of the membrane is related with actin accumulation and produces persistent motion of the cell in that direction. The random appearance and disappearance of small domains is related with amoeboid motion, where two or three pseudopods compete for a certain time. The al-

ternation of direction gives rise to random motion of the virtual cell.

Stochastic reaction-diffusion equations, as in Eqs.(1-7), and previously developed [21], can be numerically integrated into a one-dimensional domain as in the original study. Kymographs are shown next for a certain window of parameter values, the spatio-temporal dynamics of concentration R displays relatively stable patches which appear at different locations; see spatio-temporal plots in Fig. 3.

In the simulations shown in Fig. 3, the parameters k_{14} and k_{18} are kept constant and the response of P along the membrane is quite similar for the parameters considered. There are some persistent patches during a long period of the simulations. Under such conditions the cell may develop its own locomotion. Note that the activation of P by R is weak; a strong coupling, controlled by parameter k_{13} , would correlate the patches of both fields. We keep the original values of this parameter [21]. For small values of the parameter k_5 and large values of k_2 , the concentration of R is high and homogeneously distributed along the membrane; see corresponding spatio-temporal plots in Fig.3. The concentration of R increases the probability of the generation of patches of P , and therefore, depending on the particular realization, some directed motion is expected under such conditions. On the other hand, in the opposite limit, large values for parameter k_5 and small values for k_2 , the concentration of R is low, and the probability of directed motion is smaller.

If we fix k_2 and k_5 values and vary the parameters controlling for the evolution of P , we obtain the inverse behaviour; see Fig.4. For large values of k_{14} and small values of k_{18} the membrane is completely covered by P , while for small values of k_{14} and large values of k_{18} the concentration of P strongly decreases. Locomotion is, therefore, expected for intermediate values of these two parameters as shown in Fig. 4. However, the effect of changing such parameters on the dynamics of R is small.

B. Mechanism of amoeboid motion is based in bistability

For the evaluation of the mechanism of the spatio-temporal plots in Figs. 3 and 4, we fixed the stochastic source of perturbations of the additive noises in eqs (1-7) to $\sigma_R = 0.04$ and $\sigma_P = 0.025$. No changes were expected in the average behaviour or in the quantification the value of the total concentration R in the face of the parameters k_2 and k_5 because the fluctuations are additive [49]. Stationary solutions were found for the deterministic version of Eqs. (1-7). Slowly increasing the parameter k_2 we observed the evolution of the stationary value of R ; see Fig. 5. Once the system of

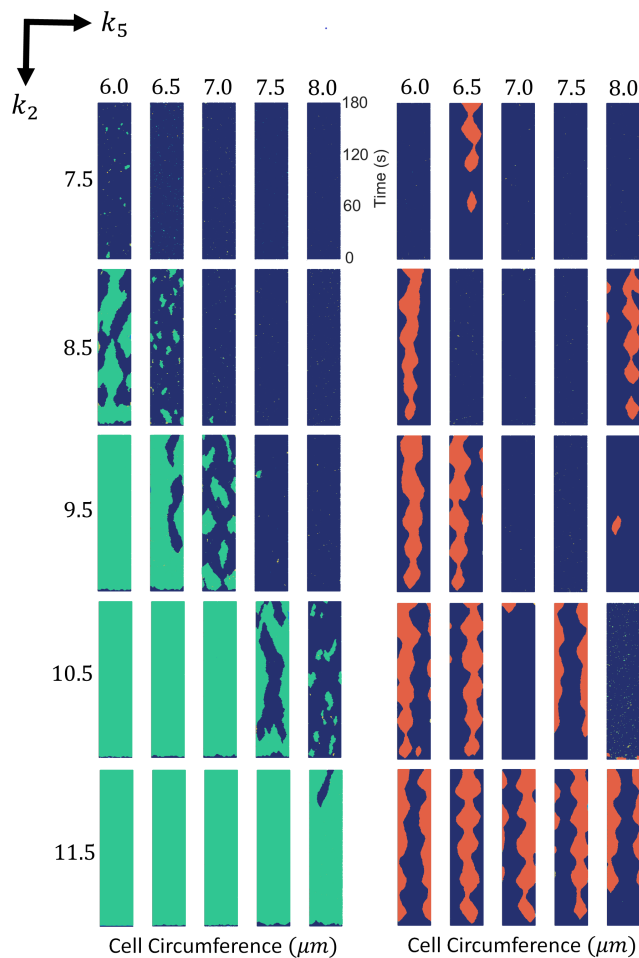


Figure 3. Spatio-temporal plots of R (in green) and P (in red) for different values of k_5 and k_2 . For each panel times goes from bottom to top and horizontal direction corresponds to membrane position in the cell circumference. Variances of noise intensity were fixed at $\sigma_R = 0.04$ and $\sigma_P = 0.025$.

equations saturated to a certain value of $R \sim 0.85 - 0.90$ we reduced the value of k_2 , giving rise to a hysteresis cycle; see Fig. 5A. The hysteresis cycle shows that the system actually follows bistable dynamics. Equivalent dynamics of R can be observed under a similar change in k_5 ; see Fig. 5B.

In contrast, the same analysis was made for the constants k_{14} and k_{18} , which are related to the variable of the pseudopod inducer P. The resulting dynamics revealed bistable behavior for two stable states as shown in the hysteresis curve for parameters k_{14} (Fig. 5C) and k_{18} (Fig. 5D).

It is known that the combination of a bistable dynamics with an appropriate noise intensity, produces the formation of localized patches in reaction-diffusion

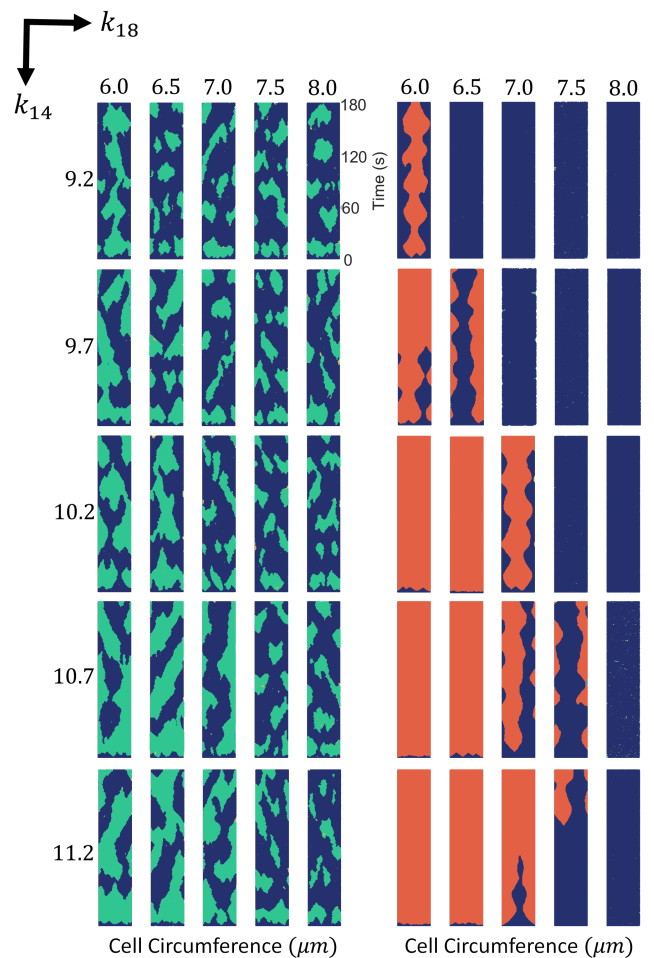


Figure 4. Spatio-temporal plots of R (in green) and P (in red) for different values of k_{14} and k_{18} . For each panel times goes from bottom to top and horizontal direction corresponds to membrane position in the cell circumference. Variances of noise intensity were fixed at $\sigma_R = 0.04$ and $\sigma_P = 0.025$.

equations [50, 51]. This formation is the mechanism responsible for the formation of localized domains of R and P. The localized pattern observed in Fig. 3 is not due to excitable dynamics but rather to bistable dynamics with noise.

C. Stochastic bistability provides a mechanism of cell crawling motion in two dimensional systems

For the coupling of the polarization mechanism to the proper cell motion shown in the previous section we used a phase field. This additional field is employed for the definition of the interior of the cell. In this case, the two dimensional phase field permits the use of different

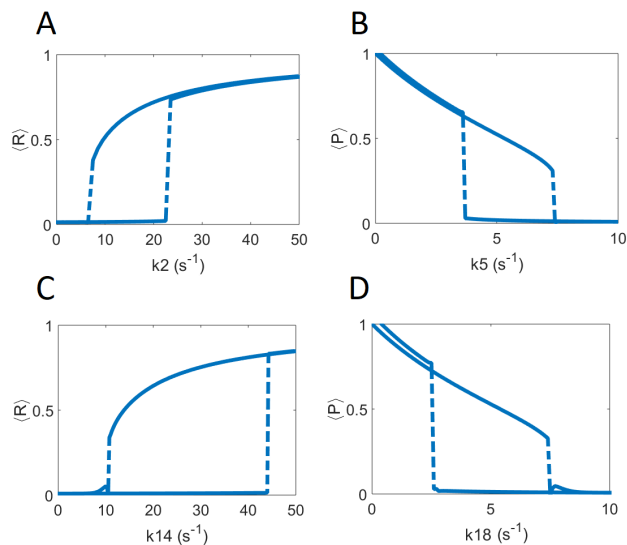


Figure 5. Hysteresis curves of the deterministic model for R dynamics varying (A) k_2 and (B) k_5 . Similar hysteresis curves of the deterministic model for P dynamics were obtained when varying (C) k_{14} and (D) k_{18} .

biochemical concentrations in the ventral part of the cell in a surface.

The extension of the stochastic reaction-diffusion described in the previous section to two dimensions permits numerical simulations of the shape of the crawling cell and the corresponding motion responding to the dynamics of the patches. In Fig. 6 we see snapshots of the *in silico* cells with different parameter values corresponding to equivalent parameter values shown in Fig. 3. We reproduced the dynamics expected from the one dimensional simulations and the crawling dynamics can be clearly studied. Again, for small values of parameter k_5 and large values of k_2 the concentration of R is mostly high and homogeneously distributed along the membrane; see Fig. 6. On the other hand, in the opposite limit, for large values of k_5 and small values of k_2 the concentration of R disappears from the ventral membrane. However, for a small window of values of the parameters the cell moves and inspects the surrounding region. The shape of the resulting cell depends on the particular realization and the parameter values; in the snapshots shown in Fig. 6 we obtain fan-shaped cells, a typical mode of *Dictyostelium discoideum* cell crawling [35].

From the snapshots resulting from Fig. 6 different scenarios show different types of movement together with the concentrations of R and P. The model exhibits sensitivity to variations in parameters k_2 and k_5 . Different realizations of simulations with the same parameters could bring the cell from quite persistent movement into

an alternation between an almost static state for low concentrations of $\langle R \rangle$, and transitory motion in random directions for large values of $\langle R \rangle$. As in Fig.3 the small influence of R in P is evident in these two-dimensional simulations. Note that the presence of patches of P appearing for high values of k_2 and low values of k_5 is more common because $\langle R \rangle$ slightly increases the probability of forming new $\langle P \rangle$ patches. In contrast, for low values of k_2 and high values of k_5 the presence of $\langle P \rangle$ patches is less frequently observed.

In contrast to this, the dependence of locomotion on the parameters k_{14} and k_{18} is much stronger as shown in Fig.7, where persistent motion is observed only for intermediate values of the two parameters. For very small or very large amounts of $\langle P \rangle$ cells do not move, independently of the behaviour of R.

D. Noise intensities determine the type of motion

The variation of the type of cell motion is determined by the intensity of the noise. Low levels of both noises do not permit the formation of the domains of R and P needed to give rise to cell movement; see Fig.8. As we increase the amplitude of noise for P, we reach a single domain that fills the front part of the cell and persistent motion is shown; see middle column and right hand snapshots in Fig.8. This type of motion is reminiscent of the fan-shaped amoeboid cells previously reported [35] and also reproduced with simpler models [36]. An increase in the noise intensity produces an increase in the appearance and disappearance of pseudopods and therefore a transition to amoeboid movement; see fifth column in Fig.8 for higher noise intensities. Another evident change the effects of which will be discussed in the following sections is the variance associated with the formation of Ras patches (σ_R) becoming varied. There are some noise intensities which produce patterns and dynamics similar to the characteristic patterns observed in the experiments, however, as previously mentioned, and shown in Fig.10, small variations in the parameter values may completely change the movement dynamics.

E. Inclusion of mass-conservation stabilizes cell motion

In order to reduce the high sensitivity of the movement on the parameter values, we included a conservation constraint on the total quantities of the protein Ras R and the inducer P in the biochemical rates responsible for the bistable transition. Following similar previous approaches [32, 45], we included this conservation as a global feedback condition in the reaction-diffusion equations.

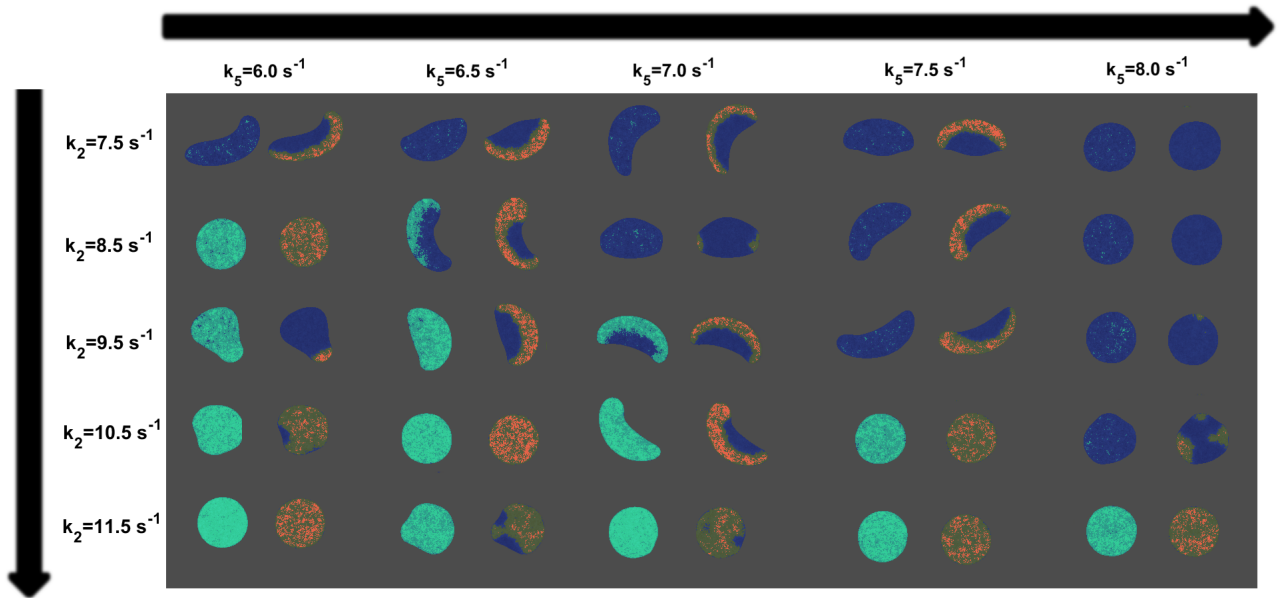


Figure 6. Snapshots of the virtual cells showing R (in green) and P (in red) obtained from computer simulations and applying the phase field technique to the model for different values of k_2 and k_5 . Variances of noise intensity were fixed at $\sigma_R = 0.04$ and $\sigma_P = 0.025$.

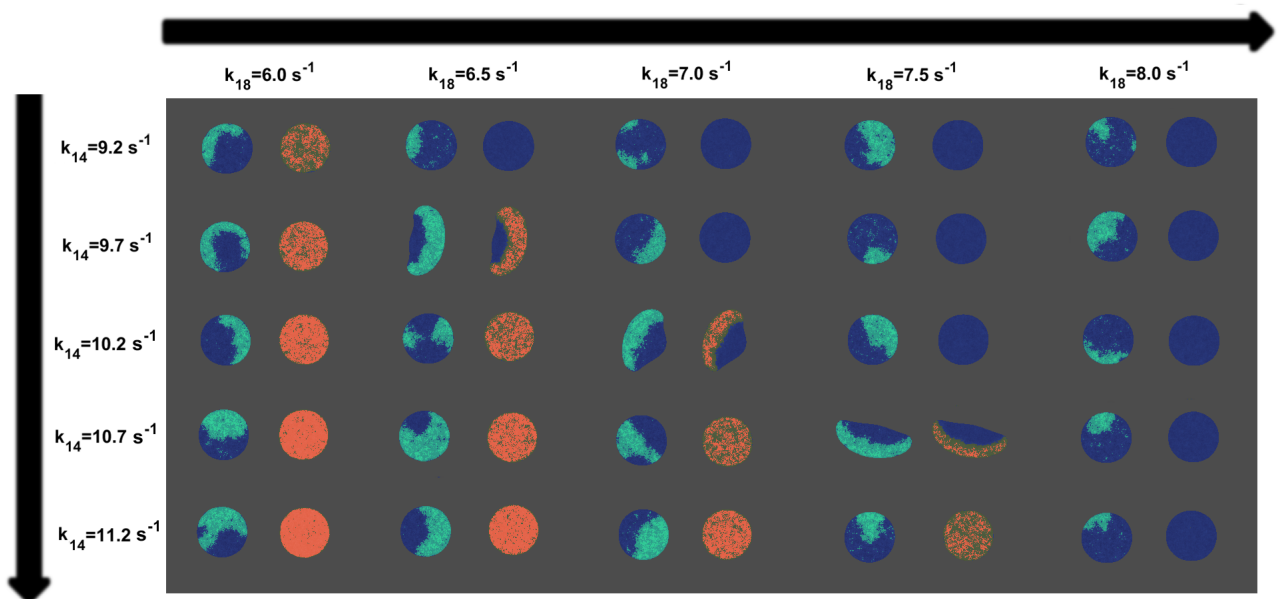


Figure 7. Snapshots of the virtual cells showing R (in green) and P (in red) obtained from computer simulations and applying the phase field technique to the model for different values of k_{14} and k_{18} . Variances of noise intensity were fixed at $\sigma_R = 0.04$ and $\sigma_P = 0.025$.

In Fig. 9 several realizations incorporating the conservation constraint of R and P proteins, for different

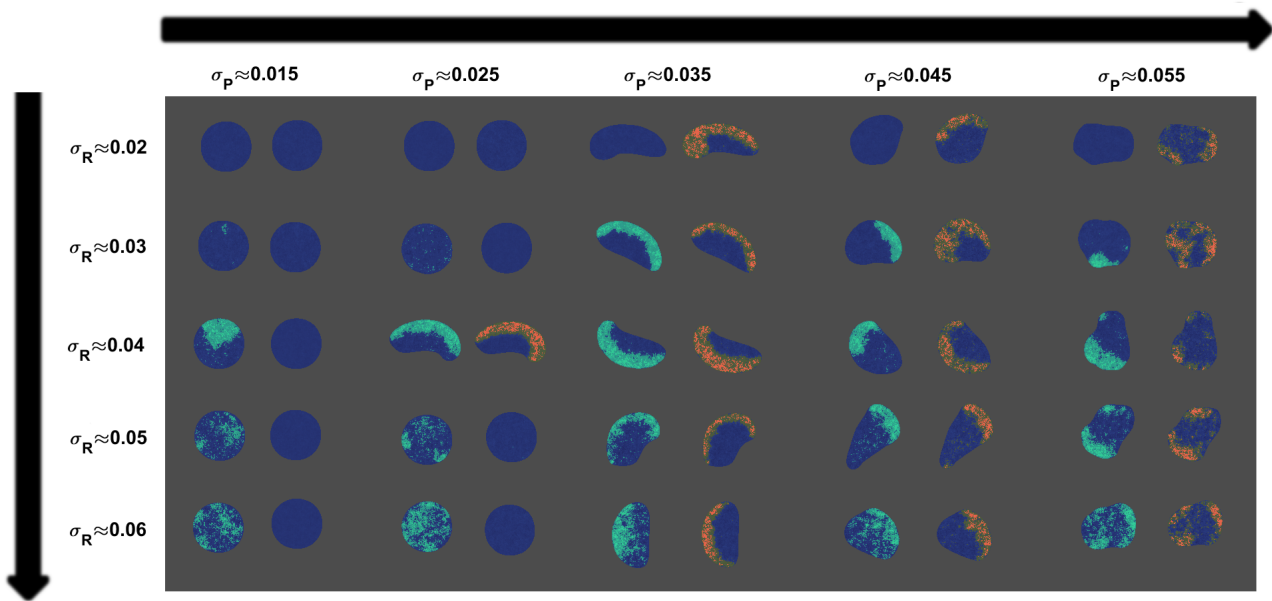


Figure 8. Map of snapshots of the virtual cell taken from different variance values of noise intensity for the original model [21]. For every column, left/green snapshots refer to R distribution while right/red snapshots indicate P distribution. The value of the parameter of the simulations are $k_2 = 9.50$, $k_5 = 7.0$, $k_{14} = 10.20$ and $k_{18} = 7.0$. The rest of them are consistent with Table 1.

parameter values are shown; see Eqs.9 and 10. A direct comparison can be made with the results displayed in Fig. 6. Results in Fig. 9 show the effects of the inclusion of the mass conservation feedback, where a wide change in the parameter values does not affect either the bistability of the model or the quantity of protein R inside the cell phase field, which was kept constant. The inclusion of this global condition permits the use of a larger range of parameter values, increasing the robustness of the mechanism in comparison with the original model.

As with the cases without mass conservation, the shape and type of motion were affected by the noise intensity. Using the same parameters of Fig. 8 we studied the effects of varying the noise variance in the new mass-conserved model. In Fig. 10 we see two different types of transitions. The first is observed when the variance related to the pseudopod inducer P increases, changing the shape from persistent fan-shape to random amoeboid phenotype. This change is present because while small values of P variance generates less blurred patches, an increment in the P variance drives the opposite effect, which is the appearance of more blurred and distributed patches for P.

For a second transition, we follow the same comparison line between the simulations without and with mass conservation from Fig. 8 and 10, respectively; now we analyze the effects for different values of the variance

corresponding to the dynamics of the Ras concentration R. Similar to the patterns of P, small values of σ_R induce the formation of less diffuse and distributed Ras patches. In contrast, greater values of σ_R stimulate more diffuse and distributed Ras patches. Despite the close relationship between the effects of σ_R and σ_P , the real difference is in the dynamics of the movement. For example, if we focus on the top of the first column of Fig. 10 for small values of the noise variances we see for both snapshots a domain in the front part of the cell which translates into persistent motion. Now, if we look in detail at the bottom of the first column corresponding to higher a value for the variance σ_R , we see a notable difference in the left hand snapshots, moving from a more compact domain in the front part of the cell to a more diffuse domain inside the cell. This transition only takes place at the Ras concentration (R) level, while maintaining consistent dynamics of the pseudopod inducer P and thus persistent motion of the cell. The same analogy could be made for the last column in Fig. 10 where high values of σ_P lead to a more random motion for all the cases regardless of the value of σ_R , the effect of which is to promote the appearance of less and more distributed Ras patches but without affecting the dynamics.

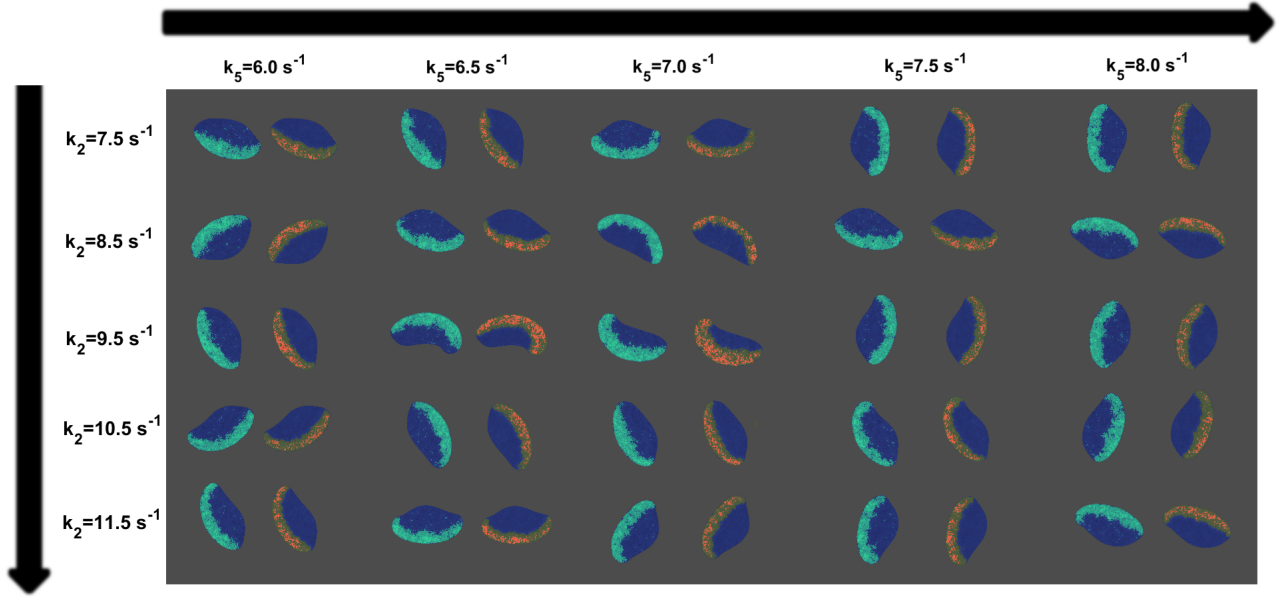


Figure 9. Map of snapshots of the virtual cell taken from different values of k_2 and k_5 for the new mass-conserved model. For every column, left/green snapshots refer to R distribution while right/red snapshots indicate P distribution. Variances of noise intensity were fixed at $\sigma_R = 0.04$ and $\sigma_P = 0.025$.

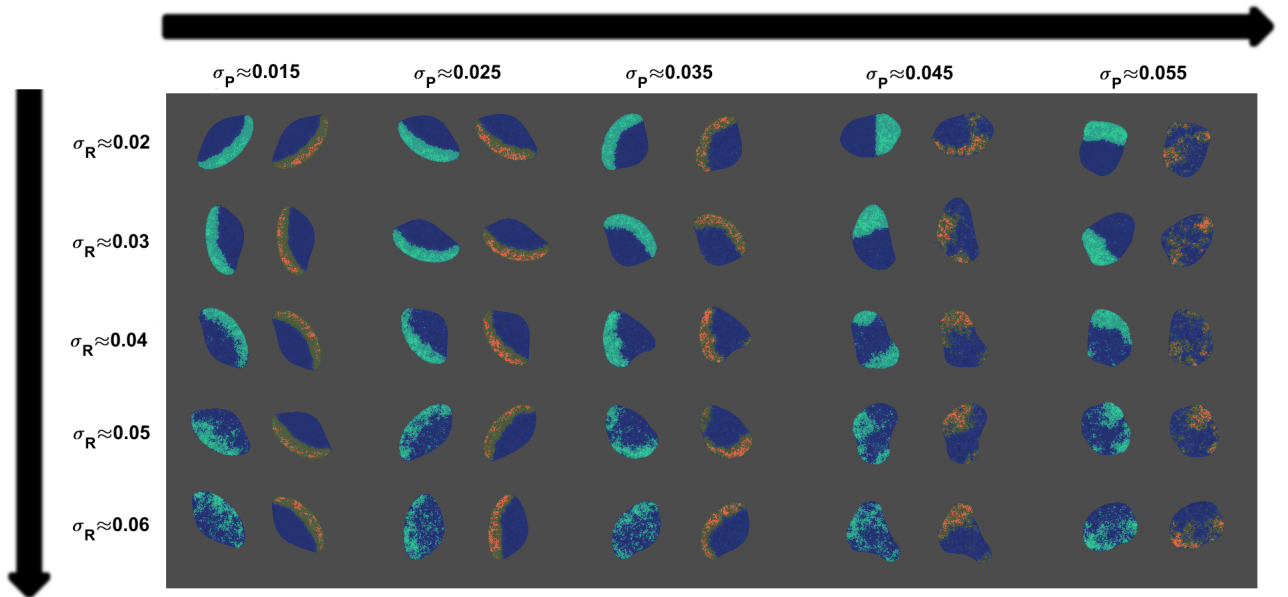


Figure 10. Map of snapshots of the virtual cell taken from different variance values of noise intensity for the new mass-conserved model. For every column, left/green snapshots refer to R distribution while right/red snapshots indicate P distribution. The value of the parameter of the simulations are $k_2 = 9.50$, $k_5 = 7.0$, $k_{14} = 10.20$ and $k_{18} = 7.0$. The rest of them are consistent with Table 1.

F. Model with mass-conservation constraint is more robust

formation on the polarization process in single cells. We

The use of the mass conservation condition has been previously employed for the generation of stable pattern

employed a version of the mechanism to modify previous reaction-diffusion equations to incorporate restrictions on the conservation of R and P. We show that this condition increases the window of parameters of the model to develop typical dynamics of cell crawling.

For the characterization of the mechanism we calculated the speed of the resulting cells for different parameter conditions for the original and the new mass-conserved models. We observed that the dynamics of the simulated cells are more robust for the mass-conserved version of the equations; see Fig. 11.

For the original model the speed and shape drastically changes when varying the parameters, and every simulation reproduces different dynamics of crawling cells (see Fig. 6). Furthermore, for the new mass-conserved version both velocities and shapes are more similar to each other for a much larger window of parameter values, as we can see in the speeds calculated in Fig. 11. Results displayed in Fig. 11A were obtained by changing k_5 to correspond to simulations shown in the third row of Figs. 6 and 9. The dynamics are fixed because of the conservation condition. In contrast, Fig. 11B was obtained by changing k_{18} to correspond to simulations shown in the third row of Figs. 7 for the no mass conservation case (results not shown for the mass-conservation system). Here one can see the preserving of the speed in the new mass-conserved system in comparison with the original model due to the small window of parameters, without the mass conservation condition that shows crawling dynamics.

In Fig. 12 we see the dependency of the speed on the noise σ_P for different values of σ_R . The speed of the cells employed for the calculation comes from the results in Figs. 8 and 10. For the outcome of the original model, which is displayed in blue bars, we do not observe a clear tendency in the bars. However, in contrast, in the new mass-conserved model results, represented by red bars, a clearer tendency in the bars is noted.

We observe that the speed obtained from the new mass-conserved model decreases for greater noise intensities. However, for the set of blue bars almost null velocities appear for low noise magnitude, and as we increase the noise variance, different values close to the magnitude of the red bars are reached, thereby showing a similarity in the speed measurements as the variance is increased.

IV. DISCUSSION

We studied the dynamics of a one-dimensional *Dictyostelium Discoideum* cell model which is mainly made up of coupled Ras activation (R), pseudopod inducer (P) and stochasticity. The deterministic model by itself reveals the emergence of bistability. This is from the visible hysteresis transition under the change of a set of

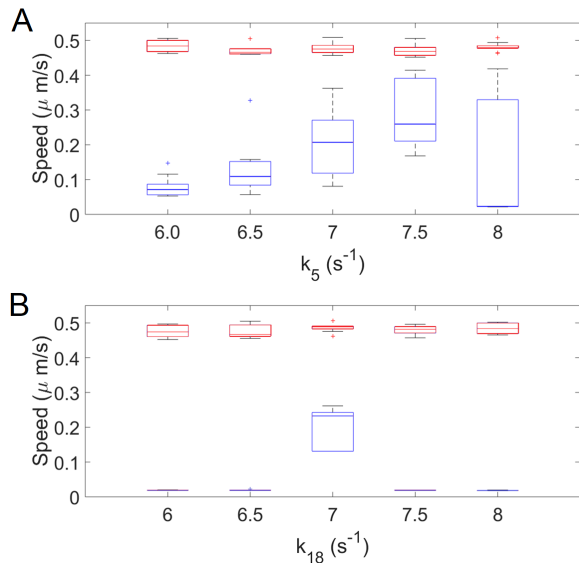


Figure 11. Box plot representation for the cell speed of the original model (blue color) and the new mass-conserved model (red color). Results are for when A) k_5 and B) k_{18} are varied. For both cases it was used a fixed value of $k_2 = 9.5$ and $k_{14} = 10.2$, $\sigma_R = 0.04$ and $\sigma_P = 0.025$. Ten realizations for each case were performed.

parameters. In contrast, the model with the stochastic part permits the transition between two stable regimes which are induced by the parameters and the noise intensity. The extension of the model into two dimensions with the use of the addition of a phase field, allowing cell deformation, shows similar behaviour when parameters are varied to the one-dimensional model, in agreement with [21].

Since for most of the realistic scenarios the mass barely changes despite environmental perturbations, we chose to incorporate global feedback for the Ras and pseudopod inducer inside the cell. This increases the robustness of the model and expands the parameter range without affecting the shape and dynamics.

Note that other global feedback were already considered in the original version of the model [21]; see the dynamics of the global inhibitors, defined by G_R and G_P in Eq.(2) and Eq.(5) respectively, similarly to other models of the motion of *Dictyostelium discoideum* cells based on global cytosolic quantities [10, 46]. The addition of global control quantities which can determine the available concentration inside the cell has previously been employed in other models [30, 36, 45].

Instant speed was measured, highlighting that for the original model a considerable set of parameters driven to velocities of close to zero, while for the set of parameters for the new mass-conserved model the speed remained almost constant.

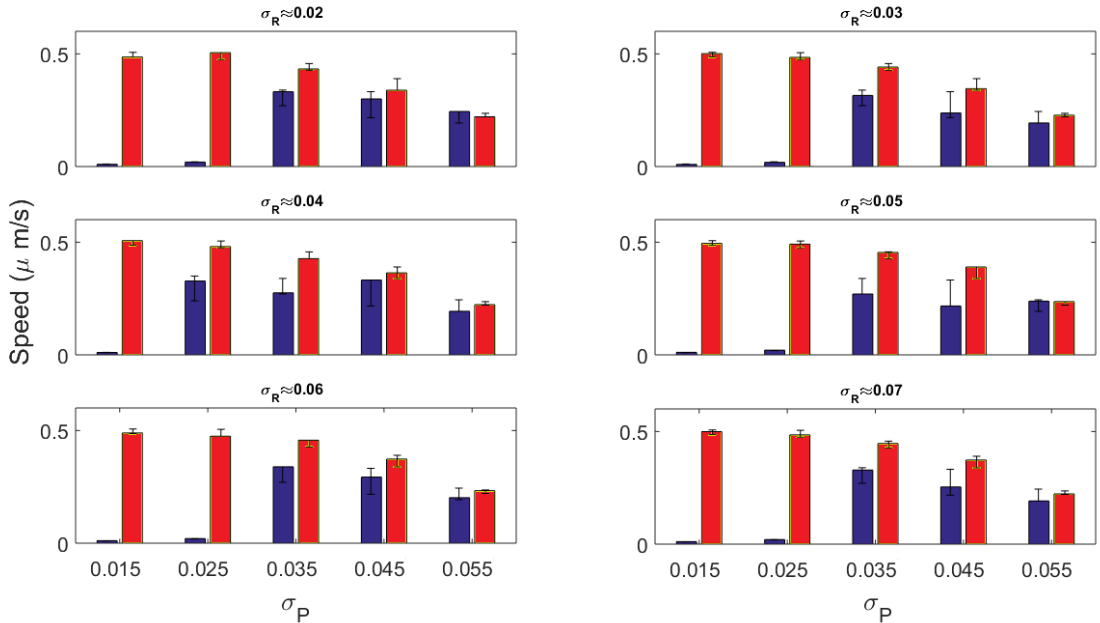


Figure 12. Speed bar plots measured by the original model (blue bars) and the new mass-conserved model (red bars) by varying the noise variance σ_P . In each panel the variance associated to σ_R was fixed for different values.

Note that we have shown that the original model is based on a bistable conditions with the appropriate noise intensity. We have previously used simple stochastic bistable models for the description of the motion of *Dictyostelium discoideum* cells [32, 36] based on the same concept together with a mass-conservation constraint. There are also other models based on similar constraints [45]. Therefore, this constraint is a convenient mechanism to increase robustness in the delicate equilibrium between stochastic fluctuations and a bistable condition.

The coupling of R on the pseudopod inducer P is weak. The coupling is produced by the term proportional to k_{13} and it increases the probability of the generation of patches of P. A chemotactic concentration can enhance R and, therefore, polarize the field P and direct the locomotion [21]. In the absence of chemotaxis the coupling is small, while more physiological conditions may require larger couplings. In Fig.13 we increased parameter k_{13} to demonstrate the increase in the coupling of both field R and P through the parameter. Intermediate values can be compared with experimental measures to fit an appropriate value; however such evaluation is outside the scope of this work.

An extension of the new mass-conserved model is possible with the inclusion of an external chemo-attractant gradient to analyze the response, known as chemotaxis and already considered in the original model [21]. Future simulations should study the relation of the chemo-

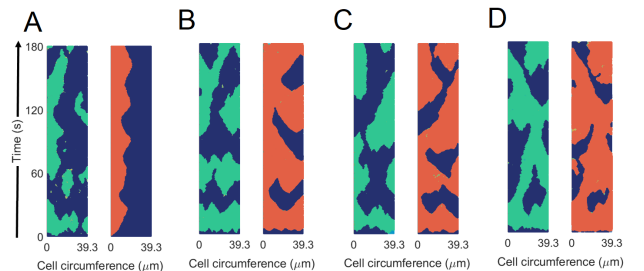


Figure 13. Spatio-temporal plots of R (in green) and P (in orange) for different values of the coupling parameter between R and P: $k_{13} = 0.1$ (A), $k_{13} = 0.50$ (B), $k_{13} = 1$ (C), and $k_{13} = 2$ (D) in the new mass-conserved model. Results are for a fixed values of $\sigma_R = 0.04$ and $\sigma_P = 0.025$.

tactic motion of *Dictyostelium discoideum* cells with the stochastic fluctuations and the rest of the parameters. They should also measure the effects on the shape and speed caused by the gradient.

In summary, we have shown that the inclusion of a mass-conservation constraint in the correct position substantially increases the robustness of a computational model of a crawling cell.

ACKNOWLEDGMENTS

We thank grant PGC2018-095456-B-I00 funded by MCIN/AEI/10.13039/501100011033 and by “ERDF A way of making Europe”, by the “European Union”. E.M. acknowledges also financial support from CONACYT.

Appendix A: Integration of stochastic partial differential equations

The Gaussian white noises employed in the model described here are always additive, and therefore it is enough to use a Euler-Maruyama method for the integration of the stochastic partial differential equations (SPDE) considered here [49]. Assuming a generic version of the equations considered here:

$$\frac{\partial C(\vec{x}, t)}{\partial t} = F(C(\vec{x}, t)) + \xi(\vec{x}, t), \quad (\text{A1})$$

the standard method to integrate this SPDE consists in the discretization in space ($\Delta\vec{x}$): from $C(\vec{x}, t)$ to $C_i(t)$, and time (Δt) and to account for the particularities of the noise terms:

$$C_i(t + \Delta t) = C_i(t) + \Delta t F(C_i(t)) + \sqrt{\frac{2\sigma^2 \Delta t}{\Delta x^d}} N(0, 1), \quad (\text{A2})$$

where d is the spatial dimensionality of the domain considered (here $d=1$ or $d=2$), and $N(0,1)$ corresponds to a random number generated by a normal distribution of mean zero and variance 1.

Such standard method for the integration of SPDE is equivalent under some conditions with the version employed in the original publication of the model [21] employed here:

$$C_i(t + \Delta t) = C_i(t) + \Delta t F(C_i(t)) + N(0, \sigma_2), \quad (\text{A3})$$

which under correct tuning of the parameter σ_2 can give rise to an equivalent description.

Appendix B: Parameters and constants used in the model.

The meaning of the biochemical parameters and of the parameters associated to the phase field can be obtained, respectively from the original studies [21] and [36].

Note also that the parameters related to a chemoattractant gradient [21] were excluded in this study.

Parameter	Value	Parameter	Value
k_0	0.01 s^{-1}	D_R	$0.75 \mu\text{m}^2/\text{s}$
k_1	1.5 s^{-1}	D_{LR}	$0.25 \mu\text{m}^2/\text{s}$
$k_2 - k_2^*$	$7.5-11.5 \text{ s}^{-1}$	D_P	$0.75 \mu\text{m}^2/\text{s}$
k_3	1.5 s^{-1}	D_{LP}	$0.25 \mu\text{m}^2/\text{s}$
k_4	1.0 s^{-1}	D_M	$0.25 \mu\text{m}^2/\text{s}$
k_5	$6.0-8.0 \text{ s}^{-1}$	n_1	2.0
k_6	0.1 s^{-1}	n_2	2.0
k_7	0.05 s^{-1}	n_3	2.0
k_9	0.15 s^{-1}	K_R	0.4
k_{10}	0.1 s^{-1}	K_P	0.4
k_{11}	0.1 s^{-1}	K_M	0.4
k_{12}	0.1 s^{-1}	σ_R	0.02 – 0.06
k_{13}	0.1 s^{-1}	σ_P	0.015 – 0.055
$k_{14} - k_{14}^*$	$9.2-11.2 \text{ s}^{-1}$	τ	$2.0 \text{ pNs}\mu\text{m}^{-2}$
k_{15}	0.5 s^{-1}	γ	2.0 pN
k_{16}	1.5 s^{-1}	ϵ	$0.75 \mu\text{m}$
k_{17}	1.8 s^{-1}	β	$18.64 \text{ pNs}\mu\text{m}^{-3}$
k_{18}	$6.0-8.0 \text{ s}^{-1}$	A_0	$122.7 \mu\text{m}^2$
k_{19}	0.1 s^{-1}	α	$10.0 \text{ pNs}\mu\text{m}^{-1}$
k_{20}	0.15 s^{-1}	C_R	$30.6 \mu\text{m}^2$
k_{21}	0.2 s^{-1}	C_P	$30.6 \mu\text{m}^2$
k_{22}	0.1 s^{-1}	η	2.0 s^{-1}
k_{23}	0.1 s^{-1}	Δt	0.03 – 0.003 s
k_{24}	0.03 s^{-1}	Δx	0.32 – 0.16 μm

-
- [1] M. C. Cross and P. C. Hohenberg, Reviews of modern physics **65**, 851 (1993).
 [2] A. Koch and H. Meinhardt, Reviews of modern physics **66**, 1481 (1994).
 [3] S. Kondo and T. Miura, science **329**, 1616 (2010).
 [4] P. Gross, K. V. Kumar, N. W. Goehring, J. S. Bois, C. Hoegge, F. Jülicher, and S. W. Grill, Nature Physics **15**, 293 (2019).
 [5] A. Mogilner, J. Allard, and R. Wollman, Science **336**,

- 175 (2012).
 [6] B. A. Camley and W.-J. Rappel, Journal of physics D: Applied physics **50**, 113002 (2017).
 [7] W.-J. Rappel and L. Edelstein-Keshet, Current opinion in systems biology **3**, 43 (2017).
 [8] A. Jilkine and L. Edelstein-Keshet, PLoS Comput Biol **7**, e1001121 (2011).
 [9] C. Beta and K. Kruse, Annual Review of Condensed Matter Physics **8**, 239 (2017).

- [10] Y. Xiong, C.-H. Huang, P. A. Iglesias, and P. N. Devreotes, *Proceedings of the National Academy of Sciences* **107**, 17079 (2010).
- [11] Y. Mori, A. Jilkine, and L. Edelstein-Keshet, *Biophysical journal* **94**, 3684 (2008).
- [12] F. Bergmann and W. Zimmermann, *PloS one* **14**, e0218328 (2019).
- [13] F. Brauns, J. Halatek, and E. Frey, *Physical Review X* **10**, 041036 (2020).
- [14] J. Halatek and E. Frey, *Nature Physics* **14**, 507 (2018).
- [15] S. Alonso and M. Baer, *Physical biology* **7**, 046012 (2010).
- [16] P. K. Trong, E. M. Nicola, N. W. Goehring, K. V. Kumar, and S. W. Grill, *New Journal of Physics* **16**, 065009 (2014).
- [17] L. Bosgraaf and P. J. Van Haastert, *PloS one* **4**, e5253 (2009).
- [18] H. Kae, C. J. Lim, G. B. Spiegelman, and G. Weeks, *EMBO reports* **5**, 602 (2004).
- [19] M. Etzrodt, H. C. Ishikawa, J. Dalous, A. Müller-Taubenberger, T. Bretschneider, and G. Gerisch, *FEBS letters* **580**, 6707 (2006).
- [20] A. T. Sasaki, C. Janetopoulos, S. Lee, P. G. Charest, K. Takeda, L. W. Sundheimer, R. Meili, P. N. Devreotes, and R. A. Firtel, *Journal of Cell Biology* **178**, 185 (2007).
- [21] P. J. van Haastert, I. Keizer-Gunnink, and A. Kortholt, *Molecular biology of the cell* **28**, 922 (2017).
- [22] C. Shi, C.-H. Huang, P. N. Devreotes, and P. A. Iglesias, *PLoS computational biology* **9**, e1003122 (2013).
- [23] C.-H. Huang, M. Tang, C. Shi, P. A. Iglesias, and P. N. Devreotes, *Nature cell biology* **15**, 1307 (2013).
- [24] I. Hecht, D. A. Kessler, and H. Levine, *Physical review letters* **104**, 158301 (2010).
- [25] I. Hecht, M. L. Skoge, P. G. Charest, E. Ben-Jacob, R. A. Firtel, W. F. Loomis, H. Levine, and W.-J. Rappel, *PLoS Comput Biol* **7**, e1002044 (2011).
- [26] M. P. Neilson, D. M. Veltman, P. J. van Haastert, S. D. Webb, J. A. Mackenzie, and R. H. Insall, *PLoS Biol* **9**, e1000618 (2011).
- [27] M. Otsuji, S. Ishihara, K. Kaibuchi, A. Mochizuki, S. Kuroda, *et al.*, *PLoS Comput Biol* **3**, e108 (2007).
- [28] B. A. Camley, Y. Zhao, B. Li, H. Levine, and W.-J. Rappel, *Physical review letters* **111**, 158102 (2013).
- [29] D. Shao, H. Levine, and W.-J. Rappel, *Proceedings of the National Academy of Sciences* **109**, 6851 (2012).
- [30] B. A. Camley, Y. Zhao, B. Li, H. Levine, and W.-J. Rappel, *Physical Review E* **95**, 012401 (2017).
- [31] M. Nickaen, I. L. Novak, S. Pulford, A. Rumack, J. Brandon, B. M. Slepchenko, and A. Mogilner, *PLoS computational biology* **13**, e1005862 (2017).
- [32] S. Alonso, M. Stange, and C. Beta, *PloS one* **13**, e0201977 (2018).
- [33] L. Stankevicius, N. Ecker, E. Terriac, P. Maiuri, R. Schoppmeyer, P. Vargas, A.-M. Lennon-Duménil, M. Piel, B. Qu, M. Hoth, *et al.*, *Proceedings of the National Academy of Sciences* **117**, 826 (2020).
- [34] N. Ecker and K. Kruse, *PloS one* **16**, e0246311 (2021).
- [35] Y. Miao, S. Bhattacharya, M. Edwards, H. Cai, T. Inoue, P. A. Iglesias, and P. N. Devreotes, *Nature cell biology* **19**, 329 (2017).
- [36] E. Moreno, S. Flemming, F. Font, M. Holschneider, C. Beta, and S. Alonso, *Physica D: Nonlinear Phenomena*, 132591 (2020).
- [37] Y. Cao, E. Ghabache, Y. Miao, C. Niman, H. Hakozaki, S. L. Reck-Peterson, P. N. Devreotes, and W.-J. Rappel, *Journal of the Royal Society Interface* **16**, 20190619 (2019).
- [38] Y. Cao, E. Ghabache, and W.-J. Rappel, *Elife* **8**, e48478 (2019).
- [39] A. Moure and H. Gomez, *Computer Methods in Applied Mechanics and Engineering* **320**, 162 (2017).
- [40] S. Flemming, F. Font, S. Alonso, and C. Beta, *Proceedings of the National Academy of Sciences* **117**, 6330 (2020).
- [41] J. Löber, F. Ziebert, and I. S. Aranson, *Scientific reports* **5**, 9172 (2015).
- [42] D. A. Kulawiak, B. A. Camley, and W.-J. Rappel, *PLoS computational biology* **12**, e1005239 (2016).
- [43] E. Moreno, R. Grossmann, C. Beta, and S. Alonso, Preprint (2021).
- [44] H. Kitano, *Towards a theory of biological robustness* (2007).
- [45] D. Imoto, N. Saito, A. Nakajima, G. Honda, M. Ishida, T. Sugita, S. Ishihara, K. Katagiri, C. Okimura, Y. Iwatake, *et al.*, *bioRxiv* (2020).
- [46] D. Taniguchi, S. Ishihara, T. Oonuki, M. Honda-Kitahara, K. Kaneko, and S. Sawai, *Proceedings of the National Academy of Sciences* **110**, 5016 (2013).
- [47] R. M. Cooper, N. S. Wingreen, and E. C. Cox, *PloS one* **7**, e33528 (2012).
- [48] P. J. van Haastert, *PloS one* **16**, e0246345 (2021).
- [49] J. García-Ojalvo and J. Sancho, *Noise in spatially extended systems* (Springer Science & Business Media, 2012).
- [50] P. Hanggi, T. J. Mroczkowski, F. Moss, and P. V. McClintock, *Physical Review A* **32**, 695 (1985).
- [51] H. A. Kramers, *Physica* **7**, 284 (1940).